

Using Synergies in Dual-Arm Manipulation Tasks

Raúl Suárez, Jan Rosell and Néstor García

Abstract—The paper deals with the problem of planning movements of dual-arm anthropomorphic systems, with the aim of reducing the computational cost of the problem and making the movements look as human-like as possible. The key idea of the proposal is the search of synergies of the dual-arm anthropomorphic system in order to use them to reduce the dimension of the search space while preserving human-like appearance. This idea was already developed and successfully used to plan movements of robotic hands, thus the extension to a dual-arm system is attractive. The paper presents a description of the proposed approach as well as real experimental results that encourage doing further research in this line.

I. INTRODUCTION

Robot motion planning is a field whose importance grows as the complexity of the robotic devices increases, being relevant in different applications from industrial manipulation to humanoid robotics [1]. In the case of humanoid robots, the goal of motion planning is twofold. On the one side, it looks for valid movements to solve a task dealing with a relatively large number of degrees of freedom (DOF), and, on the other hand, it tries to mimic the movements of human beings, sometimes with kinematic structures that are not completely equivalent.

Pursuing the first goal, different motion planners able to deal with high number of DOF have been developed, being the most frequently used the sampling-based planners like *Probabilistic Road Map planners* (PRM) [2] or *Rapidly-exploring Random Trees planners* (RRT) [3]. Several further improvements on these approaches have been proposed like, for instance, dealing with optimality [4] or constraints [5], or biasing sampling towards more promising regions of the configuration space using dynamic domains [6], workspace information [7] or Principal Component Analysis [8]. Seeking the second aim, the search for human-like movements is done by looking for proper coordination between the robot joint movements.

A typical example of this planning problem appears with robotic hands, which are devices with many DOF (several hands are available with four or five fingers with three or four DOF per finger, e.g. *Barrett Hand*, *Shadow Dextrous Hand*, *SAH* and *SDH* from *Schunk*, *H2 Compliant Hand* from *Meka Robotics*, *Gifu Hand* from *Dainichi Ltd.*, *Azurra Hand* from *Prensilia* and *Allegro Hand* from *SimLab*).

The authors are with the Institute of Industrial and Control Engineering (IOC), Universitat Politècnica de Catalunya (UPC) – Barcelona Tech, Barcelona, Spain (raul.suarez@upc.edu). This work was partially supported by the Spanish Government through the projects DPI2011-22471 and DPI2013-40882-P.

In this context, several works used the couplings between the finger joints in order to reduce the planning complexity as well as to look for human-like hand postures. The basic idea is to establish a correlation between the DOF of the robotic hand fingers equivalent to that existing in the human hand. Relevant pioneering works dealt with the grasping problem, analyzing the correlations of finger joints when the hand was grasping an object and called them “hand postural synergies” [9]. Other works used the same concept to find pre-grasp hand configurations [10], and called “eigen-grasp” to each independent hand movement involving correlated movements of all the joints. These works allow a reduction of the grasp space up to a 2-dimensional space. The study of hand synergies was also addressed recently for prototypes of specific hands [11]. The same concept was used in other works for telemanipulation purposes [12].

These works were oriented to grasp synthesis, others applied the same concept to motion planning trying to mimic human hand postures [13], in this case the correlations between the finger joints are used to determine movement directions so they were called “principal motion directions” (PMDs). Motion planning requires the determination of the correlation of the finger movements when they are freely moved trying to cover the whole hand workspace without any external constraint [14]. Other applications dealt with the synthesis of human-like motions in graphic applications [15]. Dimensionality reduction techniques based on synergies have also been used in the selection of grasping forces [16] as well as embedded in the hand control system [17][18].

The comments above, regarding the use of synergies to reduce the complexity of hand motion planning and to look for hand movements that mimic the human movements, is relevant here because the proposal in this work is the use of similar concepts applied to the motion planning of a dual-arm system with anthropomorphic features.

The number of anthropomorphic dual-arm systems available in the market has significantly grown in the last years, either as a specific product (e.g. [19]) or as a composition of manipulator arms assembled imitating a human structure (e.g. [20]). These devices typically have 12 or 14 DOF, which is a significant number when motion planning has to be done, and becomes even more relevant when the dual-arm system is part of a whole humanoid robot or when it is equipped with hands as those mentioned above.

Even when all the arm DOF may be independently moved, when a human being performs tasks with both arms in a bounded workspace some synergies exist, and looking for them is the first goal of this work. By bounded workspace

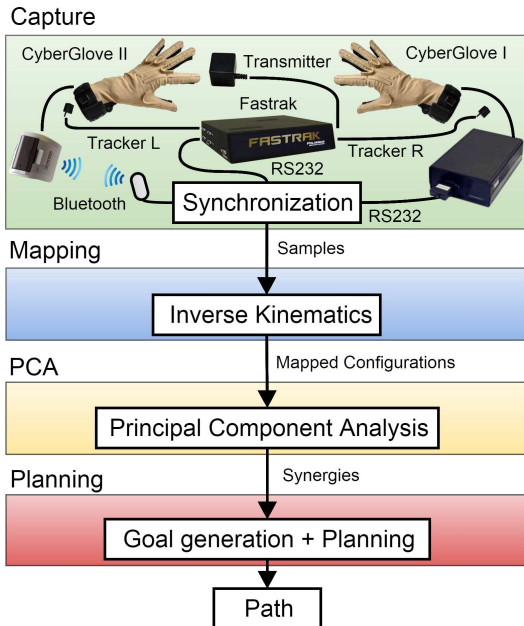


Fig. 1. General schema of the proposed approach.

we refer here to a space located in front of the body (talking about a human being) with easy visual access. We are not considering here that, for instance, the human operator has to do something in the back of his body.

After this introduction Section II presents the problem statement and gives an overview of the proposed approach; Section III describes the experimental setup and the way in which the dual-arm synergies are determined; Section IV presents the motion planner used in this work, and Section V illustrates the approach performance by showing experimental results. Finally, Section VI summarizes the approach and indicates the future work.

II. PROBLEM STATEMENT AND APPROACH OVERVIEW

As stated above, the final problem to be solved is the coordinated motion planning of a dual-arm system, and, for this, the existence of synergies in the human dual-arm system will be investigated. The proposed approach is conceptually equivalent to that used regarding hand synergies. The main steps can be summarized as follows (see Fig. 1):

- 1) The human operator performs different tasks using both hands (see Fig. 2), and the wrist configurations of both arms are sampled during the execution (i.e. the position and orientation of both hands).
- 2) The inverse kinematics of the robotic dual-arm system is computed for each pair of wrist configurations sampled in Step 1. As a result, a set of joint configurations of the dual-arm robotic system is obtained. Note that this set could be obtained by sampling the human arm joints and mapping them in some way to the robotic system, but this could be not evident when the kinematic structures are not clearly equivalent.
- 3) A Principal Component Analysis (PCA) [21] is run on the set of configurations obtained in Step 2. A new reference system of the dual-arm configuration space



Fig. 2. Human operator performing a task with both hands while wearing the measurement equipment.

is obtained, with the axis ordered according to the dispersion of the samples in a decreasing order.

- 4) A reduced number of components (those with highest dispersion) is selected to obtain a subspace that, with lower dimension, contains a high percentage of the sample set (the percentage depends on the number of selected components and therefore can be controlled). Planning the arm movements in this configuration subspace significantly reduces the complexity of the problem while the human-like appearance is preserved (within the limits allowed by the kinematics of the mechanical system). Different strategies can be used to exploit this subspace during the planning phase.

This general schema was originally applied to the motion planning of robotic hands to simplify the search of grasping configurations, as well as to plan free movements preserving the human-like appearance (e.g. [13][22]). Nevertheless, its application to an anthropomorphic dual arm systems has not been reported yet and, therefore, the results of this work lead to a generalization of the procedure to human-like dual arm systems.

It must be noted that the dual-arm configuration information can be processed in two possible ways. On one side, the information about the joints of the human arms can be captured and directly used for the PCA, in this way the real synergies of the human arms are obtained and must then be mapped in a non-trivial way to the robotic dual-arm system (see an example in [23]). On the other side, the human arm movements can be mapped first onto the robotic system, so that when the human moves the arms the movements are automatically mapped to the robotic system, and then the PCA can be applied on the resulting values of the mechanical joints. In this way the synergies are directly obtained for the used robotic system in correspondence with the movements done by the human operator. In this work the second option is used.

III. DETERMINATION OF DUAL-ARM SYNERGIES

The sampling of human configurations and their mapping to the robotic system is of vital importance in order to correctly reproduce the human synergies in the dual-arm robotic system. With this in mind, this section describes the experimental setup, the motion capture procedure, the configuration mapping, and the Principal Component Analysis.

A. Experimental setup

The experimental setup involves the following devices:

- A *robotic dual-arm system* (shown in Fig. 3a) composed of two industrial robot arms *UR5* from *Universal Robots* [24] with 6 DOF each one, which are assembled emulating the human arm configuration. Each robot is equipped with an *Allegro Hand* from *Simlab* [25] that has 16 DOF.

- Two *sensorized gloves CyberGlove* (shown in Fig. 1 and worn by the operator in Fig. 2) were used to capture the orientations of the hands of the human operator. Each glove provides 22 joint-angle measurements: three flexion sensors per finger, four abduction sensors between the fingers, a palm-arch sensor and two sensors to measure the flexion and abduction of the wrist. In the wristband there is a mounting provision for a motion tracking sensor.

- Two magnetic wrist *trackers Fastrak* from *Polhemus* with 6 DOF (shown in Fig. 1 and worn by the operator in Fig. 2), were used to capture the position and orientation of user wrists referenced to the global frame.

- A home-developed simulation tool, called *The Kautham Project* [26], that includes tools for collision detection, motion planning and graphical visualization of the whole system.

B. Sampling and mapping dual-arm configurations

In order to capture information about the movements of the operator arms, all the sensors are synchronized to take samples at the same time with a rate of 50 Hz. Each sample contains a translation vector and a rotation quaternion read from each *Fastrak* tracker, 22 measurements describing the positions of the finger joints and the hand orientation (flexion and abduction) read from each glove, a sample identification number, and information about the time when it was captured. Nevertheless, from the information provided by the gloves only the values describing each hand orientation are actually used in this work.

Once the samples from the human movements have been taken, they are mapped to the robotic system in order to obtain the corresponding configurations. This mapping is done for each arm as follows. For $i \in \{L, R\}$, let (see Fig. 3):

${}^W T_{B_i}$ be the transformation from the world reference frame (located between the two arm shoulders) to the base of arm i ,

${}^{B_i} T_{TCP_i}$ be the transformation from the base of arm i to its tool base (TCP),

${}^W T_T$ be the transformation from the world reference frame to the *Fastrak* transmitter,

${}^T T_{S_i}$ be the transformation from the *Fastrak* transmitter to the i -th tracker sensor,

${}^{S_i} T_{TCP_i}$ be the transformation from the tracker sensor i to the TCP of the arm i .

Since the configuration of the robot TCP must follow the configuration of the human wrist, the transformations from the base to the human wrist and to the robot wrist must be equivalent, i.e. it can be considered that

$${}^W T_{B_i} {}^{B_i} T_{TCP_i} = {}^W T_T {}^T T_{S_i} {}^{S_i} T_{TCP_i} \quad (1)$$

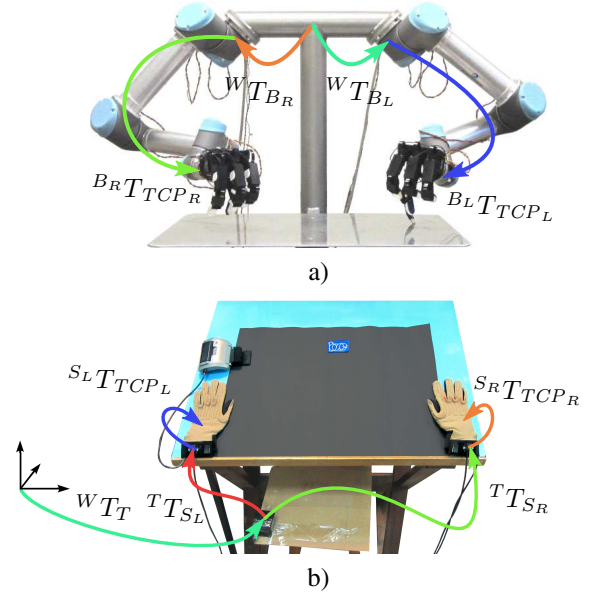


Fig. 3. Transformations related to: a) the robot arms, b) the gloves and the trackers.

and solving for ${}^{B_i} T_{TCP_i}$ results,

$${}^{B_i} T_{TCP_i} = ({}^W T_{B_i})^{-1} {}^W T_T {}^T T_{S_i} {}^{S_i} T_{TCP_i} \quad (2)$$

Note that $({}^W T_{B_i})^{-1}$ and ${}^W T_T$ are constant and known, while ${}^T T_{S_i}$ depends on the tracker information and ${}^{S_i} T_{TCP_i}$ depends on the glove information.

${}^{B_i} T_{TCP_i}$ is used to solve the arm inverse kinematics. Due to the arm structure, up to 8 different kinematic solutions can be obtained. In this work, the configuration shown in Fig. 3 is always selected (it looks visually as the most human-like posture), being the solution for each joint given by inverse kinematics in the range $[-\pi, \pi]$. It should be remarked here that all the joints of the *UR5* robot have a range $[-2\pi, 2\pi]$, therefore it is possible to adjust the values of the angles (by adding or subtracting 2π) within the total range of 4π in such a way that the samples are grouped with a minimal variance, which improves the results of the PCA. Then, after solving the inverse kinematics of both arms for all the samples, the values of the arm joints are adjusted as follows.

The average angle $\bar{\theta}_j$ of all the resulting values for each joint j is computed as¹:

$$\bar{\theta}_j = \text{atan2}(\bar{S}_j, \bar{C}_j) \quad (3)$$

$$\text{with } \bar{S}_j = \frac{1}{n} \sum_{k=1}^n \sin(\theta_{j_k}) \text{ and } \bar{C}_j = \frac{1}{n} \sum_{k=1}^n \cos(\theta_{j_k}) \quad (4)$$

where n is the number of processed samples. The function $\text{atan2}(y, x)$ is the arctangent with two arguments and its use is mandatory to get θ_j in the appropriate quadrant. The resulting average angle lies in the range $[-\pi, \pi]$. Then, the value $R_j = \sqrt{\bar{S}_j^2 + \bar{C}_j^2}$ is a measure of the distribution of values, i.e. if $\forall k \theta_{j_k} = \bar{\theta}_j$ then $R_j = 1$, and if the values

¹Note that the arithmetic mean cannot be used since it does not take into account that any angle plus $\pm 2\pi$ rad represents the same joint position.

of θ_{jk} are uniformly distributed then $R_j = 0$ and $\bar{\theta}_j$ is not defined (note that $R_j = 0$ implies that $\bar{C}_j = \bar{S}_j = 0$ and then $\text{atan2}(0,0)$ is not defined; in this case, $\bar{\theta}_j = 0$ is chosen). Finally, the average angle $\bar{\theta}_j$ of each joint j is used to adjust the joint values θ_{jk} obtained from the inverse kinematics solutions to new values $\hat{\theta}_{jk}$ as,

$$\hat{\theta}_{jk} = \begin{cases} \theta_{jk} & \text{if } |\theta_{jk} - \bar{\theta}_j| \leq \pi \\ \theta_{jk} - \text{sign}(\theta_{jk})2\pi & \text{otherwise} \end{cases} \quad (5)$$

minimizing in this way the variance of the samples.

C. Principal Component Analysis

A *Principal Component Analysis* (PCA) is run over the arm configurations of both arms resulting from the mapping. Since all the joints have the same movement range, it is not necessary to normalize the scale of the samples.

The PCA identifies the directions of the dual-arm configuration space where the samples have larger dispersion. The larger the eigenvalues, the larger the dispersion of the data along the corresponding eigenvector directions.

The vectors of the new base of the dual-arm configuration space returned by the PCA are ordered in a decreasing order according to the corresponding dispersion of the samples (i.e. the first vector indicates the direction with maximum dispersion of samples). The directions indicated by these vectors are called *Principal Motion Directions* (PMDs) and represent the arm synergies. In the rest of the paper *synergies* and PMDs will be used with equivalent meaning.

IV. PLANNER

A. PMD subspace

The planner used in this work is an RRT-Connect that is run on a subspace of the whole m -dimensional dual-arm configuration space ($m = 12$ for the dual-arm system used in this work). This subspace, called PMD subspace, is defined by a reduced number of PMDs which is chosen to cover a predefined percentage of the samples used to compute them.

B. Start and goal configurations

The goal of a manipulation task carried out by the dual-hand system can be described by the constraints affecting the poses of the objects grasped by the hands. The configurations of the objects that satisfy the goal of the manipulation task form the goal subspace, and its dimension depends on the imposed constraints (for instance, the initial relative pose for insertion of a cylindrical peg grasped by the left hand into a cylindrical box grasped by the right one has 7 DOF if the insertion can be performed anywhere in the workspace, while it has 4 if the base of the box has to lie on the table).

Once a manipulation task is defined, the goal subspace is sampled and the samples are verified to be feasible (i.e. an inverse kinematic solution exists for the robots to place the objects there without colliding with the environment or with themselves). Then, the robot configurations obtained by the inverse kinematics are kept as valid goals for the dual-arm system if: a) the distance to the PMD subspace is below a given threshold and b) the projected configuration

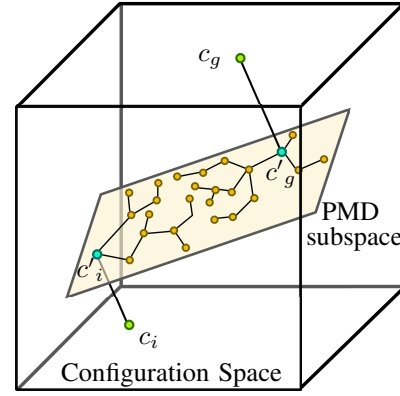


Fig. 4. Hypothetical representation of the whole task configuration space, and the PMDs subspace where the RRT works; the real initial and goal configurations (c_i and c_g) and their projections on the PMDs subspace (c'_i and c'_g) are also represented.

onto the PMD subspace and the path connecting the goal and its projection are also collision-free. The projected configurations of the valid goals are called PMD goals. It is assumed that the start configuration, its projection onto the PMD subspace (called PMD start) and the path connecting them are collision-free.

C. Planning procedure

The planning procedure to connect the PMD start to any of the PMD goals is as follows. One instance of the RRT-Connect planner [3] is launched per PMD goal, like the one shown in Fig. 4 connecting the PMD start, c'_i , to the PMD goal, c'_g , which are the configurations projected onto the PMD subspace from the initial and goal configurations, c_i and c_g , respectively. All the RRT-Connect instances run in parallel and once a solution path is found by one of them, the motion planning is stopped and all the other threads are killed.

V. EXPERIMENTAL RESULTS

A. Demonstration Task

Several experiments have been executed in order to obtain different sets of PMDs and verify their effect in the planning process. In all the cases, a human operator was asked to execute at least 30 times a given task using the arms without moving the rest of the body (this generates sets of more than 10,000 samples). To illustrate the approach, we show in this sections the results for an *assembly* task in which the human operator must grasp a cylindrical box and a soda can, and introduce the can into the box. Besides, looking for a general and practical application of the approach, we also capture the movements and obtain the PMDs when the operator freely moves both arms and hands in an unconstrained way (i.e. without performing any specific task) trying to cover the whole workspace, we will refer to this as a *free-movement* task. There is no guarantee that the operator actually covers the whole workspace, but in this way it is expected that he/she performs his/her most natural and evident movements.

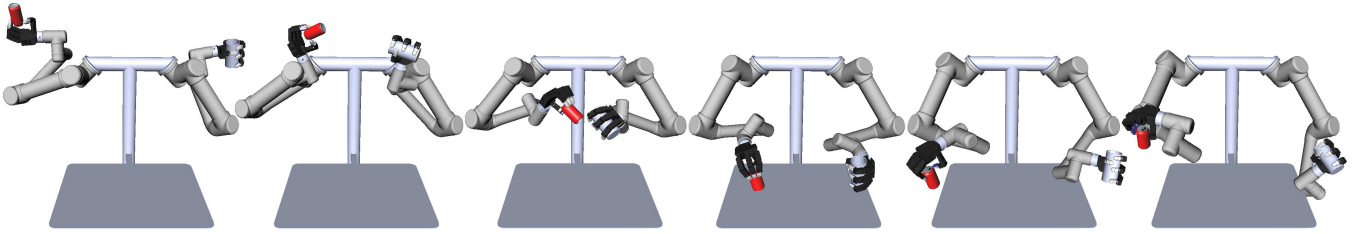


Fig. 5. Snapshots of the movements of the arms following the first PMD of the assembly task.

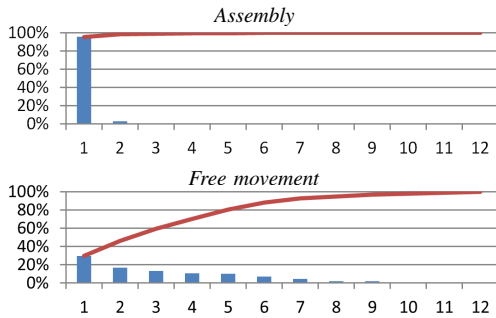


Fig. 6. Accumulated variance of samples versus the number of PMDs.

B. Obtaining the PMDs

The whole process described in Section III was applied to the tasks mentioned in Subsection V-A, and a set of PMDs was obtained in each case (i.e. a new base of the 12-dimensional space of the dual-arm configurations, with the vectors in each base ordered according to the variance of the samples along them). In order to give an illustrative example, some snapshots of the movement of the arms along the first PMD of the assembly task are shown in Fig. 5.

Table I shows the resulting variances along each PMD for each task, which are graphically represented in Fig. 6. Note that for the assembly task more than 95% of the sample variance is associated with the first PMD, while the rest of the PMDs have a very small dispersion. This means that the task executions were quite repetitive, and that the task could (almost) be done considering only one degree of freedom.

Looking to the results of the free-movement task, it can be seen that the dispersion is relevant along the first six or seven PMDs. This effect was expected since the operator has more freedom to perform the movements, which can also be seen in the total variance of the samples, clearly greater than in the assembly task (see Table I).

C. Motion planning

The assembly task described above was used to see the effect of using the PMDs in the planning phase. A RRT-Connect was run on: a) the complete 12-dimensional dual-arm configuration space, b) a 4-dimensional subspace resulting of the selection of the first four PMDs obtained specifically for the assembly task, covering 99.4% of the sample variance from the operator movements, and c) a 8-dimensional subspace resulting of the selection of the first eight PMDs obtained from the free-movement task, covering 94.7% of the sample variance from the operator movements.

TABLE I
SAMPLE VARIANCE ALONG THE j -TH PMD AND TOTAL SAMPLE VARIANCE FOR EACH TASK.

Task	Assembly		Free movements	
	var.	accumul.	var.	accumul.
1st PMD	95.4%	95.4%	29.6%	29.6%
2nd PMD	2.9%	98.3%	16.7%	46.3%
3rd PMD	0.8%	99.1%	13.2%	59.5%
4th PMD	0.3%	99.4%	10.9%	70.4%
5th PMD	0.2%	99.6%	10.2%	80.6%
6th PMD	0.1%	99.7%	7.3%	87.9%
7th PMD	0.1%	99.8%	4.7%	92.6%
8th PMD	0.1%	99.9%	2.1%	94.7%
9th PMD	0.0%	99.9%	2.0%	96.7%
10th PMD	0.0%	99.9%	1.2%	97.9%
11th PMD	0.0%	99.9%	1.2%	99.1%
12th PMD	0.0%	100%	0.9%	100%
Total [rad ²]	0.357		1.08	

In the three cases the same starting configuration of the dual-arm system and the same ten task goals were used (the number of goals was empirically selected). The ten task goals were obtained as follows, based on the procedure mentioned in Section IV. First, several potential goal configurations were generated in the physical space, i.e. configurations of the two objects to be assembled (the box and the soda can) satisfying the geometrical constraints between them necessary for the assembly operation (see Fig. 7). Note that for the assembly of the can inside the cylindrical box, the goal space is 7-dimensional, i.e. the assembly can be done in any position and orientation (six DOF) and the can can rotate around its axis while satisfying the pre-assembly pose constraints (one additional DOF). Then, these potential goals were checked to be kinematically reachable and collision free, and a set with the ten goals that have the smallest of the maximal distances to the 4-dimensional and 8-dimensional search spaces were selected (see examples in Fig. 7). In this way, the (random) set of ten goals can be used for the motion planner running in any of the three cases mentioned above.

In order to solve each of the three considered cases, an instance of the planner was run in parallel for each goal configuration, and once a valid path to solve the task was found by one the instances, the motion planner was stopped. A limit of 100 seconds and 1,000 Mbytes of memory was imposed to the executions, if the planner could not find a solution with these constraints the planner run was considered as a failure.

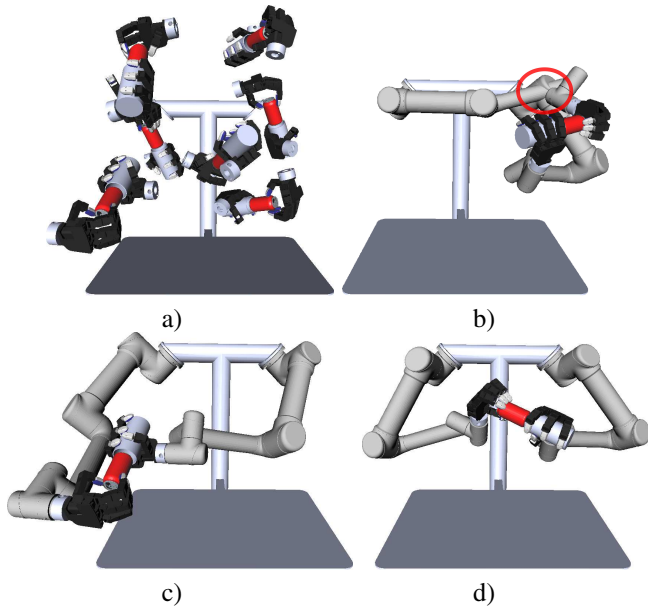


Fig. 7. Goal configurations: a) several examples in the physical space, b) not valid due to collisions, c) satisfying the assembly constraints far away from the search space, d) satisfying the assembly constraints close to the search space.

The Open Motion Planning Library (OMPL [27]) implementation of the RRT-Connect has been used encapsulated within The Kautham Project, the planning and simulation environment [26]. Table II shows the average results obtained after 100 executions per case, running in a 2.13-GHz Intel Core 2, 4-GB RAM PC. The table includes: the number of used PMDs, the dimension of the search space, the success rate, the used memory until arriving a solution, the time needed to find a solution, the length of the solution evaluated as the summation of the joints movements in radians, and the percentage of valid segments out of all the segments that were checked for validity in the RRT. Fig. 8 shows one of the solution paths obtained for the assembly task in each of the three considered cases.

From the experimental results the following can be stated:

- The use of PMDs increases the probability of obtaining collision-free configurations (fewer auto-collisions occur), thus reducing the computation time.
- The use of PMDs lowers the dimension of the search space, which lowers the number of nodes and edges of the tree and hence reduces the memory requirements.
- The use of PMDs results in motions that look more like the human motions.
- The above three results are more pronounced when task specific PMDs are used, but for general applications the utility of PMDs obtained with the free-movement task is still evident, since they also improve the results compared with planning without using PMDs.

VI. DISCUSSION AND FUTURE WORK

The paper has proposed original work dealing with the search and use of synergies of an anthropomorphic dual-arm

TABLE II
AVERAGE RESULTS OF THE MOTION PLANNING.

case	(a) without PMDs	(b) with task specific PMDs	(c) with other PMDs
used PMDs	0	4	8
space dimension	12	4	8
success rate (%)	100	100	100
used memory (Mb)	63.36	28.64	48.56
used time (s)	2.66	0.35	1.35
solution length (rad)	21.40	4.99	13.49
valid segments (%)	20	69	42

system. The approach has been implemented and an example was presented to illustrate the proposed ideas.

The concept of synergies has previously been successfully applied to anthropomorphic robotic hands, but the application to the arm's behavior was not considered before. This work opens the field towards two main aspects, one is the simplification of the planning procedure for dual-arm systems (in the same way as it was previously done for the hands) as it was shown in the paper, and the other is the possibility of classifying the tasks according to the resulting synergies, which will allow further improvements in the planning time as well as in the similarity with the human actions.

Direct future work is related with a deep analysis of different tasks that can be done with a dual-arm system, in such a way that a taxonomy or clusters of tasks could be done using the PMDs (synergies) to define a "distance" among them. Those tasks with similar systems of PMDs could be addressed and treated in similar way for motion planning purpose, thus improving the planning performance. The extension of the proposed concepts to arms forming a closed kinematic chain, e.g. when moving an object grasped by both hands, in another interesting topic for future work.

REFERENCES

- [1] J. Latombe. *Robot motion planning*. Kluwer Academic Pub., 1991.
- [2] L. E. Kavraki, P. Svestka, J. Latombe, and M. Overmars. Probabilistic Roadmaps for Path Planning in High-Dimensional Configuration Spaces. In *Proc. IEEE Int. Conf. Robotics and Automation*, pages 566–580, 1996.
- [3] J. J. Kuffner and S. LaValle. RRT-Connect: An efficient approach to single-query path planning. In *Proc. of the IEEE Int. Conf. on Robotics and Automation*, pages 995–1001, 2000.
- [4] S. Karaman and E. Frazzoli. Sampling-based algorithms for optimal motion planning. *International Journal of Robotics Research*, 30(7):846–894, June 2011.
- [5] M. Stilman. Global manipulation planning in robot joint space with task constraints. *IEEE Transactions on Robotics*, 26(3):576–584, 2010.
- [6] A. Yershova, L. Jaille, T. Simeon, and S. LaValle. Dynamic-Domain-RRTs: Efficient Exploration by Controlling the Sampling Domain. In *Proc. IEEE Int. Conf. Robotics and Automation*, pages 3856–3861, 2005.
- [7] J. Zucker, M. Kuffner and J. Bagnell. Adaptive workspace biasing for sampling-based planners. In *Proc. IEEE Int. Conf. Robotics and Automation*, pages 3757–3762, 2008.
- [8] J. Rosell, R. Suárez, and A. Pérez. Path planning for grasping operations using an adaptive pca-based sampling method. *Autonomous Robots*, 35(1):27–36, 2013.
- [9] M. Santello, M. Flanders, and J. F. Soechting. Postural hand synergies for tool use. *Journal of Neuroscience*, 18(23):10105–10115, 1998.

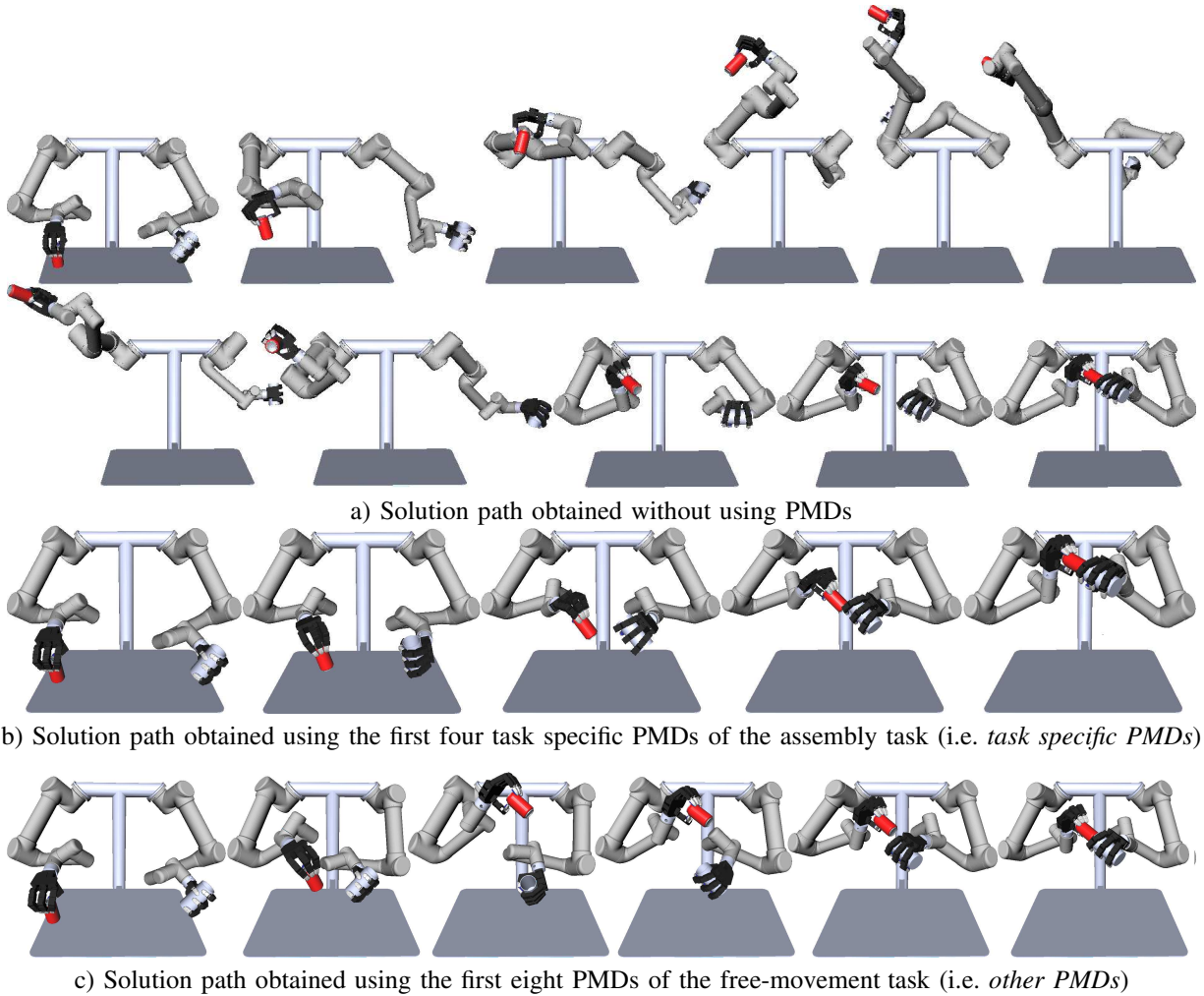


Fig. 8. Examples of valid paths obtained with the planner for each of the three considered cases.

- [10] M. T. Ciocarlie and P. K. Allen. Hand Posture Subspaces for Dexterous Robotic Grasping. *The International Journal of Robotics Research*, 28(7):851–867, July 2009.
- [11] F. Ficuciello, G. Palli, C. Melchiorri, and B. Siciliano. Postural synergies of the ub hand iv for human-like grasping. *Robotics and Autonomous Systems*, 62(4):515–527, 2014.
- [12] A. Tsoli and O. C. Jenkins. 2D subspaces for user-driven robot grasping. In *RSS Workshop on Robot Manipulation: Sensing and Adapting to the Real World*, Atlanta, GA, June 2007.
- [13] J. Rosell, R. Suárez, C. Rosales, and A. Pérez. Autonomous motion planning of a hand-arm robotic system based on captured human-like hand postures. *Autonomous Robots*, 31(1):87–102, 2011.
- [14] S. Sun, C. Rosales, and R. Suárez. Study of coordinated motions of the human hand for robotic applications. In *Proc. of the IEEE Int. Conf. on Information and Automation*, pages 776–781, 2010.
- [15] A. Safonova, J. K. Hodgins, and N. S. Pollard. Synthesizing physically realistic human motion in low-dimensional, behavior-specific spaces. *ACM Transactions Graph.*, 23(3):514–521, 2004.
- [16] M. Gabbicini, A. Bicchi, D. Prattichizzo, and M. Malvezzi. On the role of hand synergies in the optimal choice of grasping forces. *Autonomous Robots*, 31:235 – 252, 2011.
- [17] T. Wimböck, B. Jan, and G. Hirzinger. Synergy-level impedance control for a multifingered hand. In *Proc. IEEE Int. Conf. on Intelligent Robots and Systems*, pages 973–979, 2011.
- [18] G. Palli, C. Melchiorri, G. Vassura, U. Scarcia, L. Moriello, G. Berselli, A. Cavallo, G. De Maria, C. Natale, S. Pirozzi, C. May, F. Ficuciello, and B. Siciliano. Dexmart hand: Mechatronic design and experimental evaluation of synergy-based control for human-like grasping. *The International Journal of Robotics Research*, 33(5):799–824, 2014.
- [19] Rethink Robotics. <http://www.rethinkrobotics.com/products/baxter/> Baxter, June 2014.
- [20] A. Albu-Schöffer, S. Haddadin, Ch. Ott, A. Stemmer, T. Wimböck, and G. Hirzinger. The DLR lightweight robot: design and control concepts for robots in human environments. *Industrial Robot: An International Journal*, 34(5):376 – 385, 2007.
- [21] I. T. Jolliffe. *Principal Component Analysis*. Springer Series in Statistics, Upper Saddle River, NJ, USA, 2002.
- [22] J. Rosell and R. Suárez. Using hand synergies as an optimality criterion for planning human-like motions for mechanical hands. In *Proc. of the 2014 IEEE-RAS Int. Conf. on Humanoid Robots*, 2014.
- [23] G. Gioioso, G. Salvietti, M. Malvezzi, and D. Prattichizzo. Mapping synergies from human to robotic hands with dissimilar kinematics: An approach in the object domain. *IEEE Transactions on Robotics*, 29(4):825–837, 2013.
- [24] Universal Robots. UR5. <http://www.universal-robots.com/>, June 2014.
- [25] Simlab. Allegro hand. <http://www.simlab.co.kr/Allegro-Hand.htm>, June 2014.
- [26] J. Rosell, A. Pérez, A. Aliakbar, Muhayyuddin, L. Palomo, and N. García. The Kautham Project: A teaching and research tool for robot motion planning. In *IEEE Int. Conf. on Emerging Technologies and Factory Automation, ETFA'14*, 2014.
- [27] I. A. Şucan, M. Moll, and L. E. Kavraki. The Open Motion Planning Library. *IEEE Robotics & Automation Magazine*, 19(4):72–82, December 2012.